



1 **Divergent climate feedbacks in the growing period and the dormancy period to**  
2 **sowing date shift of winter wheat in the North China Plain**

3 Fengshan Liu<sup>1,2</sup>, Ying Chen<sup>1</sup>, Nini Bai<sup>1</sup>, Dengpan Xiao<sup>4</sup>, Huizi Bai<sup>4</sup>, Fulu Tao<sup>2,3,\*</sup>,  
4 Quansheng Ge<sup>2,3,\*</sup>

5 1. China National Engineering Research Center of JUNCAO Technology, Forestry  
6 College, Fujian Agriculture and Forestry University, Fuzhou 350002, China

7 2. Key Laboratory of Land Surface Pattern and Simulation, Institute of Geographic  
8 Sciences and Natural Resources Research, CAS, Beijing 100101, China;

9 3. College of Resources and Environment, University of Chinese Academy of Sciences,  
10 Beijing 100049, China

11 4. Institute of Geographical Sciences, Hebei Academy of Sciences, Shijiazhuang 050011,  
12 China

13

14 Author: Liu Fengshan, PhD, specialized in agricultural meteorology and regional climate  
15 change. E-mail: liufs.11b@igsnr.ac.cn

16 \* Corresponding author

17

18 **Abstracts:** The land cover and management changes have strong feedbacks to climate  
19 through surface biophysical and biochemical processes. Agricultural phenology dynamic  
20 exerted measurable impacts on land surface properties, biophysical process and climate  
21 feedback in particular times at local/regional scale. But the responses of climate feedback  
22 through surface biophysical process to sowing date shift in the winter wheat ecosystem  
23 have been overlooked, especially at winter dormancy period. Considering the large



24 cultivation area, unique surface property and phenology shift of winter wheat in the North  
25 China Plain, we first validated the SiBcrop model. Then, we used it to investigate the  
26 dynamics of leaf area index (LAI) and canopy temperature ( $T_c$ ) under two planting date  
27 scenarios (Early Sowing: EP; Late Sowing: LP) of winter wheat at 10 selected stations.  
28 Finally, the surface energy budget was analyzed and interpreted. The results showed that  
29 the SiBcrop with a modified crop phenology scheme better simulated the seasonal  
30 dynamic of LAI,  $T_c$ , phenology, and surface heat fluxes. Earlier sowing date had higher  
31 LAI with earlier development than later sowing date. But the response of  $T_c$  to sowing  
32 date exhibited opposite patterns during the dormancy and active growth periods: EP led  
33 to higher  $T_c$  (0.05 K) than LP in the dormancy period and lower  $T_c$  (-0.2K) in the growth  
34 period. The highest difference (0.6 K) between EP and LP happened at the time when  
35 wheat was sown in EP but wasn't in LP. The higher LAI captured more net radiation with  
36 lower surface albedo for warming, whilst surface energy partitioning exerted cooling  
37 effect. The relative contributions of albedo-radiative process and  
38 partitioning-non-radiative process determined the climate effect of sowing date shift. The  
39 spatial pattern of the climate response to sowing date was influence by precipitation and  
40 air temperature. The study highlight that the climate effects of the sowing date shift in  
41 winter dormancy period are worthy of attention.

42 **Key words:** sowing date, canopy temperature, phenology, leaf area index, winter wheat,  
43 land surface model, North China Plain

44



45 **1. Introduction**

46 Land-atmosphere interactions are key components of the climate system. The land  
47 cover and management changes have strong feedbacks with climate through surface  
48 biophysical and biochemical processes (Mahmood et al. 2014). Cropland surface  
49 characteristic had been and will continue to be changed through agricultural management,  
50 such as cropping system (Jeong et al. 2014; Cui et al. 2018), sowing date and phenology  
51 shifts (Sacks et al. 2011; Richardson et al. 2013), and bio-geoengineering (Seneviratne et  
52 al. 2018), to keep high yield under climate change condition. The changed surface  
53 properties in farmland further generate feedback to regional climate through surface  
54 energy partitioning and albedo ( $\alpha$ ) mechanisms (Cooley et al. 2005; Zhang et al. 2015). It  
55 is important to quantify the climate feedback of crop phenology shift for regional climate  
56 prediction and agriculture sustainable development.

57 There are evidences that crop phenology has been shifts substantially in the major  
58 cultivation areas worldwide (Sacks and Kucharik 2011; Tao et al. 2012; Tao et al. 2014;  
59 Liu et al. 2017). In the North China Plain (NCP), the dates of seeding, dormancy,  
60 green-up, anthesis, and maturity in wheat system were changed by 1.5, 1.5, -1.1, -2.7, and  
61 -1.4 days/decade (a positive value indicates delay and a negative value indicates advance),  
62 respectively. The vegetative stages (including periods from dormancy to greenup,  
63 greenup to anthesis) was shortened and reproductive stage was prolonged (Xiao et al.  
64 2013). The main contributors including climate change and crop management. Global  
65 warming induced-higher temperature resulted in longer photosynthetic-active period but  
66 faster development rate and shorter growth stages. Crop management reduced the lengths  
67 of vegetative stage, but increased the length of reproductive stage (Liu et al. 2010; Liu et



68 al. 2018). The phenology change is beneficial for high-yielding. The strategies adapting  
69 to warmer environment include adopting cultivars with higher accumulated growing  
70 degree days (GDD) and later planting. The prolonged grain-filling period of winter wheat  
71 benefits the accumulation of organic matter in grain (Reynolds et al. 2012; Liu et al.  
72 2018), and the adjusted sowing date reduces the risks such as insect and viral infection,  
73 adverse meteorological conditions, and soil depletion, et al.(Sacks et al. 2010). Model  
74 simulation indicated that yield increase of winter wheat was benefitted from cultivars  
75 renewal by 12.2-22.6% and fertilization management by 2.1-3.6%; climate change  
76 damaged yield by -15.0% for rain-fed type, in the NCP (Xiao et al. 2014).

77 The phenology shifts change the seasonal rhythm of crop development and affect the  
78 greenness coverage of land surface and energy and water exchanges in the boundary layer.  
79 For example, maize growth duration prolonged and reached maturity and senesced a  
80 couple of weeks later, and the maximum change can reach  $47 \text{ W m}^{-2}$  and  $-20 \text{ W m}^{-2}$  for  
81 latent heat flux ( $LH$ ) and sensible heat flux ( $SH$ ), respectively, when the NDVI is  
82 increased by 0.1 in the Agro-IBIS model (Bagley et al. 2015). Earlier planting date and  
83 longer grain-filling period increased (decreased) the  $LH$  ( $SH$ ) by 0.3 (0.2) mm/year in  
84 June and enhanced the net radiation ( $R_n$ ) in October by reducing the interval time from  
85 maturity to harvest in American maize belt (Sacks and Kucharik 2011). The change of  
86 surface coverage also shows a certain regional climate feedback. The increased spring  
87 surface greenness at farmland, due to the advanced re-greening stage of winter wheat  
88 (Xiao et al. 2013; Liu et al. 2017), significantly impacted the patterns of  $LH$  and  $SH$  and  
89 then the changes of moderate to light rainfall (Zhang et al. 2015). Harvest shifted the key  
90 influence factors of the radiative balance and evaporative fraction from leaf area and



91 soil-atmosphere temperature difference to soil moisture in U.S. winter wheat (Bagley et  
92 al. 2017), and warming future atmosphere by 1~1.4 °C through decreasing  
93 evapotranspiration in the NCP (Cho et al. 2014). So, the influence of phenology on  
94 climate feedback through surface biophysical process at local/regional scale is worthy of  
95 further studies (Liu et al. 2017).

96 Despite previous studies showed the critical role of crop phenology dynamic to  
97 surface energy and water balance, there is an important potential sensitive period that has  
98 been ignored in the winter wheat system. During the dormancy period in winter,  
99 aboveground canopy of winter wheat remained constant for more than 2 months (Xiao et  
100 al. 2013). In view of the close relationships between surface biophysical processes and  
101 surface characteristic (Boisier et al. 2012; Chen et al. 2015; Liu et al. 2017), the length  
102 from sowing date to start of dormancy would be the determinant factor to surface  
103 biophysical process in winter where winter wheat widely distributed, such as NCP,  
104 Pacific Northwest (Wuest 2010) and Southern Great Plains of USA (Bagley et al. 2017),  
105 Australia, and numerous countries surrounding the Mediterranean Sea (Mahdi et al. 1998;  
106 Schillinger 2011). Compared with climate feedback of other phenology dynamics, such  
107 as earlier re-greening stage(Xiao et al. 2013; Zhang et al. 2013), longer reproductive  
108 period (Sacks and Kucharik 2011) and inter-cropping period (Cho et al. 2014; Bagley et  
109 al. 2017), the effects of sowing date on land surface characteristic in dormancy period of  
110 winter wheat and other winter crops are relatively indirect and the effects last longer.  
111 Recognition of the impacts of sowing date on land surface characteristics and climate  
112 feedback would be beneficial to the understanding of human influence on climate change.  
113 Therefore, it is necessary to investigate whether dormancy period of winter wheat is

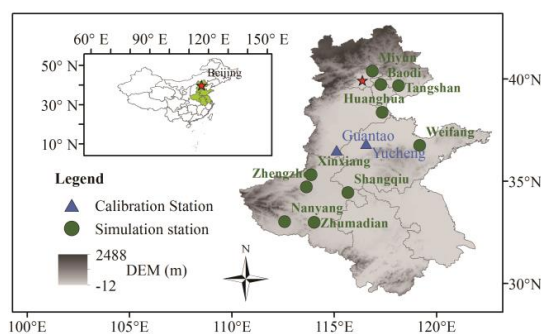


114 sensitive to sowing date. And if so, how sensitivities are surface biophysical process and  
115 climate effect?

## 116 2. Data and methods

### 117 2.1. Study stations

118 The NCP is the largest winter wheat production region in China, including Hebei,  
119 Henan, Shandong, Jiangsu, and Anhui provinces, and Beijing and Tianjin municipalities  
120 (Fig.1). Summer maize - winter wheat rotation is the main cropping system, except  
121 Anhui and Jiangsu where winter wheat-rice rotation system is dominated. Two stations  
122 with surface fluxes were used for model calibration (Fig.1, blue triangles). Ten randomly  
123 distributed stations with complete meteorology and phenology information were selected  
124 for this study (Fig.1, green dots). The natural conditions and agricultural production level  
125 of the selected stations are typical to the NCP. The stations maintain good records on  
126 both meteorological and winter wheat phenology data since 1981.



127

128 **Fig.1** Distribution map of the study area and observation sites.

129 The 30 m resolution digital elevation model (DEM), provided by the GlobeLand30 in  
130 2010, and the administrative map were download from the National Catalogue Service  
131 For Geographic Information.

### 132 2.2 Data



133 **2.2.1 Meteorology**

134 The quality-controlled meteorological data, including air temperature ( $T_a$ ),  
 135 precipitation ( $P$ ), atmosphere pressure, relative humidity, and wind speed was obtained  
 136 from the Chinese Meteorological Administration. Summer monsoon climate dominates  
 137 the region with an uneven distribution of annual precipitation (Table 1). In the 1980-2012,  
 138 the average annual  $P$  at the selected stations ranged between 550-990 mm, mainly  
 139 happened in summer. The mean yearly  $T_a$  varied between 11-15 °C. In the growing  
 140 season of winter wheat (11-12 and 1-6 month), the  $T_a$  varied between 7-11 °C among  
 141 stations and  $P$  ranged between 170-420 mm. Meteorological data was also used to drive  
 142 the model in the selected 10 stations (Fig.1).

143 **Table 1** Climate conditions of the selected stations in 1980-2012

	Station	Jan.	Feb.	Mar.	Apr.	May	Jun.	Jul.	Aug.	Sept.	Oct.	Nov.	Dec.	Average Wheat Season
$T_a$ (°C)	Baodi	-5	-1.4	5.3	13.6	19.5	24	26.1	24.8	19.8	12.7	3.7	-2.7	7.1
	Huanghua	-3.4	-0.2	5.9	14.1	20.3	25	26.9	25.8	21.2	14.2	5.5	-1.2	8.3
	Miyun	-5.9	-2.2	4.8	13.5	19.6	24	25.8	24.5	19.3	12	3	-3.7	6.6
	Nanyang	1.6	4.4	9.1	15.8	21.2	25.5	27	26	21.7	16.1	9.4	3.5	11.3
	Shangqiu	0.1	3.1	8.3	15.1	20.6	25.4	26.9	25.7	21.1	15.3	8.1	2	10.3
	Tangshan	-4.8	-1.3	5.1	13.4	19.4	23.7	25.9	25	20.3	13	4.1	-2.5	7.1
	Weifang	-2.8	0.1	5.8	13.2	19.2	23.9	26.2	25.2	20.7	14.4	6.4	-0.3	8.2
	Xinxiang	0	3.3	8.7	15.8	21.2	25.8	27	25.9	21.3	15.3	7.9	1.8	10.6
	Zhengzhou	0.5	3.5	8.7	16	21.5	26	27.1	25.7	21.2	15.5	8.4	2.5	10.9
	Zhumadian	1.5	4.2	9	15.7	21.2	25.7	27.2	25.9	21.6	16.3	9.6	3.6	11.3
$P$ (mm)	Baodi	2.7	3.7	9	20.1	36.2	82.4	169.7	142.6	49.7	27.5	10.1	3.6	167.8



Huanghua	3.2	5.5	10.1	21.3	42.8	84.2	177.2	111.6	41.5	31	11.9	3.5	182.5
Miyun	2.2	4	9.7	19.9	43.1	86.7	180.7	172.6	62.9	25.5	9.4	2.3	177.3
Nanyang	13.2	15.6	35.2	41.7	78.8	124.5	183.7	131.7	76.3	51.1	30	12.8	351.8
Shangqiu	14.3	16.3	29.3	33	65	85.2	166.8	144.8	68.5	38.2	23.4	12.7	279.2
Tangshan	3.5	4.1	9.4	22.4	47	83.2	169.7	154.3	50.8	28.2	9.5	3.4	182.5
Weifang	6	10.3	14.9	24.5	45.4	80	136.5	132.1	56.1	32.8	18.8	8.9	208.8
Xinxiang	4.6	7.1	19.2	25	49.9	65	150	119.5	59.8	32	14.9	5	190.7
Zhengzhou	9.6	12.4	27.1	30.9	63.6	67.8	146.6	134.7	75.6	40.5	21.1	9.1	241.6
Zhumadian	21.9	24.8	51	50.9	93	128.6	227.7	176.3	98.2	63.9	35.2	18.5	423.9

144  $T_a$  means air temperature, and  $P$  means precipitation.

### 145 2.2.2 Verification data

146 To verify the applicability of the model, surface flux data was collected from  
147 Yucheng and Guantao stations (Fig.1; Table 2). The two stations used the same eddy  
148 covariance instruments to measure the surface latent heat flux (LI7500, LI-COR Inc.,  
149 Lincoln, NE, USA) and sensible heat flux (CSAT-3, Campbell Scientific Inc., Logan, UT,  
150 USA), but at different heights (Yucheng:3.3 m; Guantao: 15.6 m). The post-processing  
151 software (Yucheng: Eddypro; Guantao: EdiRe) was used to process the raw data such as  
152 spike detection, lag correction of H<sub>2</sub>O/CO<sub>2</sub> relative to the vertical wind component, sonic  
153 virtual temperature correction, coordinating rotation using the planar fit method,  
154 corrections for density fluctuation (WPL-correction), and frequency response correction  
155 (Liu et al. 2011). The REddyProc was used for gap-filling by method of the look-up table  
156 and the mean diurnal variations method (Falge et al. 2001; Wutzler et al. 2018). More  
157 details could be referred to (Lei et al. 2010; Liu et al. 2013). Totally 10 complete winter  
158 wheat season flux data were used to validate the model (Table 2).



159 The meteorology conditions were also synchronously measured during flux  
160 observation (Table 2). The measurement included  $T_a$ ,  $P$ , atmosphere pressure, relative  
161 humidity, wind speed, and sunshine. These data was the inputs of the model. According  
162 to the  $T_a$  and  $P$ , the meteorological conditions were similar between the 10 stations for  
163 simulation and the two stations for calibration. More variables were observed at Yucheng  
164 station, such as wheat phenology and leaf area index (LAI) and canopy temperature ( $T_c$ ).  
165 The observed durations of phenology, LAI, and fluxes at Yucheng station were in  
166 2003-2006, 2004-2006, and 2003-2010, respectively.

167 **Table 2** General information about model verification data

Station	Period	Wheat growing season		Measured variables
		$T_a$ (K)	$P$ (mm)	
Yucheng	2003-2010	282.15	226.7	Meteorology, Phenology, LAI, $LH$ , $SH$ , $T_c$
Guantao	2008-2010	282.75	134.4	Meteorology, $LH$ , $SH$

168  $T_a$  means air temperature,  $P$  means precipitation, LAI means leaf area index ( $\text{m}^2 \text{m}^{-2}$ ),  
169  $LH$  means latent heat flux ( $\text{W m}^{-2}$ ),  $SH$  means sensible heat flux ( $\text{W m}^{-2}$ ).  $T_c$  means the  
170 simulated canopy temperature (K).

171

### 172 2.2.3 Phenology of winter wheat

173 The phenology information was manually recorded and available in the period of  
174 1981-2009, except for 2003 at Zhumadian and 1986 and 1988 at Miyun station (Table 3).  
175 Phenological statistics showed that the sowing time of winter wheat is generally between  
176 DOY (Day Of Year) 270-290 (early and middle October) in the NCP. After sowing, it  
177 generally takes about 6-10 days for germination. Winter wheat dormancy stage generally  
178 begins in December and ends in late February and early March, and reaches maturity in



179 mid-June. The standard deviation shows that the inter-annual fluctuations of dormant and  
 180 re-greening period is larger, and harvest period is relatively stable.

181 For the past 30 years, winter wheat phenology at some stations showed a significant  
 182 linear trend (Table 4). The sowing and germination periods were significantly delayed in  
 183 4 out of 10 stations, and the trend in the dormant and re-greening period was not obvious.  
 184 Winter wheat matured significantly earlier at five stations. Generally, the autumn and  
 185 winter phenophases, including sowing, germination and dormancy, are mainly delayed,  
 186 while spring and summer phenophases, including re-greening and maturity, are  
 187 primarily advanced. According to the fitting coefficient ( $a$ ), the duration were changed by  
 188 5.7, 8.1, 4.9, -3.5, and -5.5 in the period of 1981-2009, respectively, for the stages of  
 189 sowing, germination, dormancy re-greening and maturity of winter wheat. These results  
 190 were consistent with previous studies (Tao et al. 2012; Xiao et al. 2013; Xiao et al. 2015),  
 191 and indicating that the selected stations were good representation of the NCP.

192

193 **Table 3** General information on the phenology of winter wheat in the selected stations  
 194 (unit: DOY)

Station	Period	Sowing	Germination	Dormancy	Re-greening	Maturity
Baodi	1981-2009	272.83±4.33	281.55±5.5	335.62±6.86	59.19±42.72	165.97±2.57
Huanghua	1981-2009	274.17±7.83	280.32±7.03	340.38±8.65	62.45±6.56	157.14±3.25
Miyun	1981-2009	275.52±7.55	284.96±9.03	331.93±6.41	73.59±15.1	168.26±3.46
Nanyang	1981-2009	297.21±7.81	306.83±9.03	7.54±14.64	48.22±8.9	149.21±4.99
Shangqiu	1981-2009	287.59±4.07	295.31±4.79	359.21±32.4	47.03±6.43	151.59±2.99
Tangshan	1981-2009 (except 2003)	271.86±4.83	279.59±6.04	335.55±6.6	66.62±7.98	169.97±3.23



Weifang	1981-2009	274.1±5.75	284.62±17.93	343.72±7.76	59.59±7.29	160.41±3.42
Xinxiang	1981-2009	283.59±4.21	291.64±5.14	351.9±10.56	47.55±7.16	152.03±3.3
Zhengzhou	1981-2009	289.76±5.67	298.45±6.65	360.5±14.08	44.21±7.43	151.34±3.88
Zhumadian	1981-2009 (except 1986, 1988)	289.54±9.33	298.29±11.11	5.46±10.35	49.15±6.84	146.21±4.76

195 the data was shown in average ± standard deviation.

196

197

**Table 4** Linear trends in winter wheat phenology

Station	Sowing		Germination		Dormancy		Re-greening		Maturity	
	a	p	a	p	a	p	a	p	a	p
Baodi	0.31	0.00	0.41	0.00	0.14	0.36	-0.67	0.52	-0.05	0.35
Huanghua	0.18	0.31	0.17	0.31	0.38	0.05	-0.07	0.64	-0.13	0.07
Miyun	0.62	0.00	0.69	0.00	0.17	0.27	-0.51	0.15	-0.20	0.01
Nanyang	-0.18	0.30	-0.11	0.60	-0.13	0.71	0.12	0.60	-0.38	0.00
Shangqiu	0.03	0.77	0.04	0.68	0.39	0.59	0.10	0.51	-0.07	0.28
Tangshan	0.41	0.00	0.51	0.00	0.43	0.00	-0.29	0.11	-0.20	0.00
Weifang	0.20	0.11	0.61	0.13	0.11	0.55	0.14	0.38	-0.12	0.11
Xinxiang	0.07	0.46	0.12	0.34	0.27	0.26	-0.16	0.33	-0.12	0.10
Zhengzhou	-0.16	0.21	-0.21	0.17	-0.28	0.41	0.11	0.52	-0.25	0.00
Zhumadian	0.49	0.02	0.56	0.02	0.21	0.37	0.02	0.89	-0.36	0.00

198 a was the coefficient of linear fitting equation (d/year); p was the significance level

## 199 2.3 Methods

### 200 2.3.1 Model calibration and verification



201 The SiBcrop model was selected in this study. SiBcrop is a process-based land  
202 surface model adapted from the Simple Biosphere model version 3 (Lokupitiya et al.  
203 2009). The SiB series models (version 1, 2, 3 refers to SiB1, SiB2, SiB3, respectively) are  
204 widely adopted land surface model for computing surface energy, water, momentum and  
205 CO<sub>2</sub> exchange in the boundary layer. The SiBcrop version added the simulation of maize,  
206 soybean, winter and spring wheats cropping system (Lokupitiya et al. 2009). The  
207 crop-specific submodel replaces remotely-sensed NDVI information by simulated LAI  
208 and the fraction of photosynthetically active radiation. SiBcrop simulated fast response  
209 processes that vary sub-hourly such as energy, water, carbon and momentum balance of  
210 the canopy and soil, as well as the processes that vary daily such as LAI. Surface energy  
211 and water fluxes are calculated at each time step on a grid cell basis according to  
212 physiologically based formulations of leaf-level photosynthesis, stomatal conductance  
213 and respiration (Farquhar et al. 1980; Collatz et al. 1990).

214 The model was first modified according to the actual situation of winter wheat in the  
215 NCP (Chen et al. 2020). The SiBcrop model was originally calibrated in winter wheat –  
216 summer fallow system in which the growth time of wheat is relative abundant  
217 (Lokupitiya et al. 2009). However, the NCP is dominated by winter wheat – summer  
218 maize system in which the development of wheat is strictly restricted. There are great  
219 differences in the varieties, planting date, growth environment and physiological  
220 characteristics of winter wheat between the two systems. The modifications including: (1)  
221 the sowing date was postponed to October from original August. (2) The cold tolerance  
222 was reduced to 8°C from original 18°C, above which the seven consecutive days for  
223 wheat sowing was counted. (3) The harsh condition of delayed sowing also reduced the



224 daily growth rate, which was modified from 0.07 to 0.03 g m<sup>-2</sup> when GDD was 105-310  
225 °C d. (4) Wheat grows faster when GDD is 769-1074 °C d with maximum dry weight  
226 increased from 8 to 12 g and daily rate enlarged from 0.015 to 0.15 g m<sup>-2</sup>. (5) Specific  
227 leaf area was changed from 0.02 to 0.025 m<sup>2</sup> g<sup>-1</sup> (Najeeb et al. 2016). (6) A subroutine  
228 was added to describe the senescence process of canopy when GDD was larger than 1074  
229 °C d according to Tao et al. (Tao et al. 2009). More details could be referred to Chen et al  
230 (2020).

### 231 **2.3.2 Model simulation**

232 Two simulations with different sowing dates were performed to examine the  
233 responses of surface biophysical processes to shifts in sowing dates at the selected 10  
234 stations (Fig.1). The planting date was classified into two scenarios: after DOY 265 (early  
235 sowing scenario, EP) and after DOY 275 (late sowing scenario, LP). The early and late  
236 sowing scenarios were established by artificially limiting the starting time of the sowing  
237 date. The early sowing scenario means that the sowing will not be allowed until DOY  
238 265. Similarly, the late sowing scenario is only allowed after DOY 275. In both scenarios,  
239 wheat was sowed at the seventh consecutive days when temperature ranged 5~25°C,  
240 which means the real sowing date was seven days later.

241 The simulations were driven by the same meteorological data, initial condition, and  
242 soil texture from 1980 to 2009. The 1980-1984 was not analyzed as the spin-up time. The  
243 difference in the simulation results was mainly ascribed to the sowing date. The analyses  
244 focused on the dynamics of LAI and  $T_c$ , and the surface energy balance components such  
245 as  $R_n$ ,  $LH$ , and  $SH$ , which was used to explain the climate feedback mechanism.

### 246 **2.3.3. Methods to relate the surface energy balance components with $T_c$**



247 The Boisier method (Boisier et al. 2012) was adopted to relate the surface energy  
248 balance components with  $T_c$ . The energy partitioning of a terrestrial surface is expressed  
249 as

$$250 \quad (1-\alpha) S_d + L_d - L_u = LH + SH + R \quad (1)$$

251 Where  $S_d$ ,  $L_d$ , and  $L_u$  are the downward short-wave radiation, downward long-wave  
252 radiation, and upward long-wave radiation, respectively. In order to have a closed surface  
253 energy balance, the residual term  $R$  was derived explicitly from the other terms in  
254 equation (1), and principally accounts for the soil heat flux and canopy storage flux.

255 The  $T_c$  change simulated by model is affected by both radiative (surface albedo  
256 effect) and non-radiative processes (surface energy partitioning effect). In order to  
257 separate temperature variation caused by the sole change in absorbed short-wave  
258 radiation (radiative process), the following equation (Boisier et al. 2012) was used:

$$259 \quad \Delta T_c = (\varepsilon\sigma)^{-1/4} \left[ (L_u + \Delta L_u)^{1/4} - L_u^{1/4} \right] \quad (2)$$

260 Where  $\Delta T_c$  is the anomaly of canopy temperature (K). The  $\sigma$  is Stefan-Boltzmann  
261 constant ( $=5.67 \times 10^{-8} \text{ W m}^{-2} \text{ K}^{-4}$ ). The  $\varepsilon$  is surface emissivity ( $= 1$ ). A disturbance in  $S_d$ ,  
262  $L_d$ ,  $LH$ ,  $SH$  or  $R$  can be expressed as  $\Delta L_u$  by fixing non-perturbed terms using equation  
263 (1). More details can be found in Boisier et al. (2012).

264

## 265 **3 Results**

### 266 **3.1 SiBcrop simulation accuracy**

267 The SiBcrop model had been modified to improve the simulation accuracy of wheat  
268 growth and surface fluxes in our previous study (Chen et al. 2020). After modifications,  
269 the simulated biases were within 10 days for wheat emergency and harvest dates, the



270 determination coefficient, root mean square error, and agreement index between  
271 simulated and observed LAI were obviously improved from 0.26, 1.89 m<sup>2</sup> m<sup>-2</sup>, and 0.7 to  
272 0.80, 0.99 m<sup>2</sup> m<sup>-2</sup>, and 0.91, respectively. And they were 0.66, 32.37 W m<sup>-2</sup>, and 0.84,  
273 respectively, for the simulated *LH* (Chen et al. 2020).

274 The simulation accuracy for  $T_c$  was analyzed by comparing the observation with  
275 simulation at Yucheng station over 2003-2010 (data not shown). The linear regression  
276 equation (simulated  $T_c = 1.02 * \text{measured } T_c - 4.22$ ,  $R^2 = 0.91$ ,  $p < 0.001$ ) showed good  
277 linear relationship between the simulated  $T_c$  and the observed  $T_c$ . The coefficients of  
278 linearly fitted equations indicating that the simulated  $T_c$  was slightly higher than the  
279 measured (slope =1.02) and was negative deviated (intercept =-4.22). So the model can  
280 well simulate the dynamic of  $T_c$  with relatively smaller error. In this paper, we focused on  
281 the  $T_c$  difference between two sowing dates, which could reduce the influence of low  
282 numerical simulation value.

283 The simulation error for wheat phenology at Yucheng station was within 10 days  
284 (Chen et al. 2020). The sowing time under the two sowing scenarios was further  
285 compared with observation at the selected 10 stations. The simulated sowing date was  
286 stable, generally around  $\text{DOY}278.66 \pm 1.15$ , and  $\text{DOY } 290.34 \pm 2.08$  for EP and LP  
287 scenario, respectively. The observed phenology fluctuated greatly. Wheat was prone to  
288 sow later or early generally due to geographical location at some specific stations. In the  
289 EP scenario, the stations in the north had a positive difference compared to the actual  
290 phenological period, whereas the stations in the south had a negative difference, because  
291 the stations in the north had earlier sowing date than those in the south. In the LP scenario,  
292 the stations in the south were relatively close to the actual phenology, but the stations



293 near the north had a larger positive difference. Overall, the simulation difference of  
294 phenology was within 15 days. The selected scenario covers the actual situation of winter  
295 wheat sowing in the NCP. The comparisons improved the representativeness and  
296 reliability of the simulation results.

297 **Table 5** The difference between simulated and observed sowing dates under two  
298 scenarios at each station

Station	Scenario	
	Early sowing	Late sowing
Baodi	6.59±4.62	19.59±4.49
Huanghua	4.41±8.02	16.31±7.55
Miyun	4.19±7.82	17.48±7.55
Nanyang	-19.07±7.87	-8.41±8.08
Shangqiu	-9.34±3.84	1.48±3.85
Tangshan	7.41±4.95	20.38±5.47
Weifang	4.34±5.6	15.86±5.55
Xinxiang	-5.31±4.24	5.59±4.24
Zhengzhou	-11.41±5.47	-0.38±5.53
Zhumadian	-11.36±8.91	-0.57±9.07
All	-2.98±10.96	8.7±11.66

299 data was show in average ± standard deviation.

300

301 **3.2 Seasonal dynamics of LAI and  $T_c$  in scenarios**



302 Wheat LAI curves for the two sowing dates were obviously not overlapped (Fig.2a).  
303 The LAI in the EP scenario was larger with earlier development. With the sowing in the  
304 LP scenario, LAI difference between the two scenarios gradually narrowed until the  
305 spring of the next year when the disparity increased again (Fig.3a). The LAI difference  
306 between two scenarios had a valley after the reproductive period. With the approaching  
307 of harvest, the difference gradually decreased to 0.

308 The LAI difference of winter wheat in two scenarios is mainly attributed to the  
309 difference in the accumulation of organic matter. In the EP scenario, earlier sowing  
310 means advanced assimilation process and better temperature conditions, more  
311 photosynthetic carbon was produced and distributed into leaf. The impact of sowing time  
312 on LAI displayed great dissimilarity among stations (Fig.3a). Based on linear regression,  
313 the seasonal average of wheat LAI difference between scenarios was highly related with  
314 precipitation in the growth period ( $\text{LAI anomaly} = 0.0011 * P - 0.12$ ,  $R^2 = 0.59$ ). The  
315 more precipitation, the greater influence of sowing date on growth. The  $T_a$  contributed  
316 little to the LAI difference between the two scenarios.

317 The most obvious disparity in  $T_c$  between two scenarios occurred in the period when  
318 wheat had been sown in the EP but hadn't in the LP (Fig.2b). The development of early  
319 sown winter wheat resulted in higher  $T_c$ , with a peak of up to 0.6 K. The growth of wheat  
320 in the LP sharply reduced the warming effect in EP, and eventually the EP scenario had  
321 lower temperatures (-0.2K) before entering the dormancy period. The temperature change  
322 process during this period was relatively consistent across the selected stations (Fig.3b).

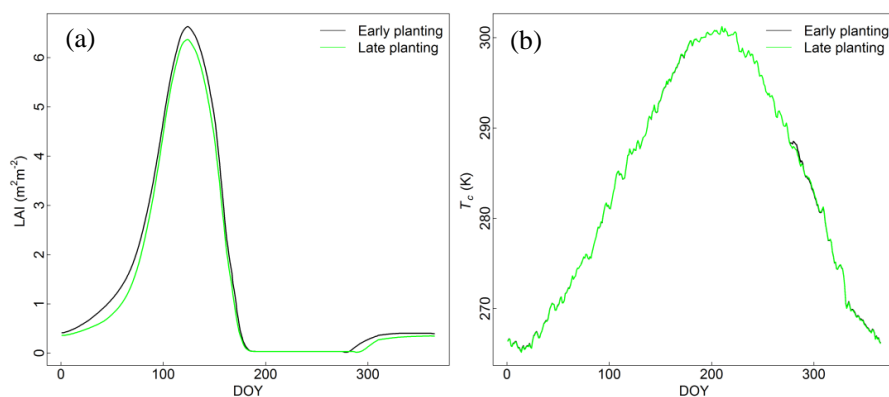
323 Another special period is the dormancy period, when EP had higher  $T_c$  than LP with  
324 average of 0.05 K (Fig.3b). With the start of the re-greening period, the EP  $T_c$  was



325 gradually lower than LP  $T_c$  and dropped to 0 at the harvest time. The  $T_c$  dynamics during  
326 this period was highly heterogeneous among the stations, varying between -0.25~0.25 K.

327 In the dormancy period, the  $T_c$  anomaly between scenarios was significantly affected  
328 by the  $T_a$  in winter ( $T_c$  anomaly =  $-0.023 * T_a + 0.062$ ,  $R^2 = 0.6$ ,  $p = 0.005$ ). The lower the  
329  $T_a$ , the bigger the  $T_c$  difference, which indicating that the influence of sowing date is  
330 more important in northern farmland. The linear relationship between  $P$  and  $T_c$  difference  
331 in winter was not obvious. The linear fitting equation between  $P$  and  $T_c$  anomaly in the  
332 growing period:  $T_c$  anomaly =  $-0.0013 * P + 0.057$ ,  $R^2 = 0.8$ ,  $p < 0.001$ . So more rainfall  
333 increased the  $T_c$  anomaly in the growing period. The linear fitting equation between  $T_a$   
334 and  $T_c$  anomaly in the growing period:  $T_c$  anomaly =  $-0.017 * T_a + 0.2$ ,  $R^2 = 0.53$ ,  $p =$   
335  $0.01$ . Since the  $T_c$  anomaly was negative, the higher the  $T_a$ , the greater the  $T_c$  anomaly.  
336 Considering the low temperature and less precipitation at the northern stations, the high  
337 temperature and more precipitation at the southern stations, the climate feedback of  
338 sowing date shift was more obvious in winter in the northern areas, and in the growing  
339 period in the southern areas.

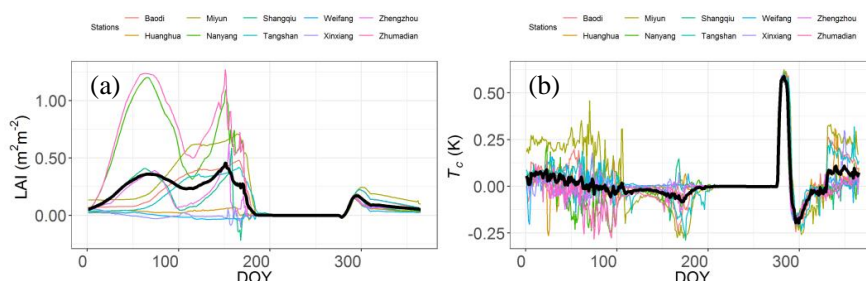
340



341



342 **Fig.2** Dynamics of (a) LAI and (b)  $T_c$  under two sowing scenarios in winter wheat  
343 growing season



344

345 **Fig.3** Seasonal differences in (a) LAI and (b)  $T_c$  of EP-LP at each station. The  
346 average across the stations was shown in bold black line

347

### 348 3.3 Contributions of surface energy balance components to scenario difference in $T_c$

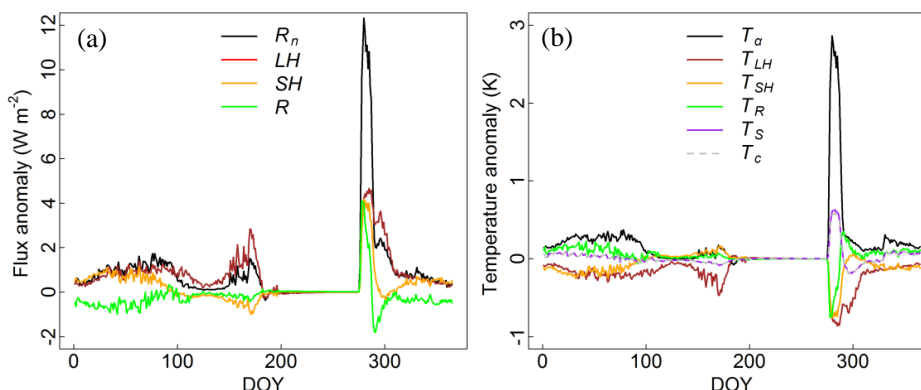
349 According to the seasonal dynamics of LAI and  $T_c$ , winter wheat growth could not  
350 explain the difference in climate effect of sowing time. Specifically, the  $T_c$  anomaly  
351 between the two scenarios were reversed between the dormancy (December, January, and  
352 February) and active growth periods (other wheat development period with active  
353 physiological activity), but with both positive LAI difference (Fig.3). In this section,  
354 surface energy balance was used to explain the response of  $T_c$  to sowing date.

355 The flux anomalies of  $R_n$ ,  $LH$ ,  $SH$  and  $R$  were shown in Fig.4a. The EP scenario  
356 always maintained higher  $R_n$  and  $LH$ . Especially winter wheat-covered ground captured  
357 more than  $10 \text{ W m}^{-2}$   $R_n$  than bare land. The anomaly of  $R_n$  in different sowing dates was  
358 maintained within  $2 \text{ W m}^{-2}$ .  $LH$  generally was covariant with the change in  $R_n$ . However,  
359 the anomaly of  $LH$  in the late growth period was greater than that of  $R_n$ , resulting in  
360 negative  $SH$ , indicating that the EP scenario had stronger  $LH$  distribution tendency and



361 less  $SH$  was partitioned. Bigger anomaly of  $SH$  was happened in the initial and dormant  
362 stages.  $R$  anomaly fluctuated obviously only in the initial phase.

363 The contributions of surface energy balance components to  $T_c$  were shown in Fig.4b.  
364 Stronger radiation absorption provided more energy for the thermal motion of air and  
365 causing positive  $T_c$  differences of EP-LP. Correspondingly, higher distribution into  $LH$ ,  
366  $SH$ , and  $R$  was conducive to cooling  $T_c$ . Therefore, positive  $LH$  and  $SH$  differences of  
367 EP-LP showed negative  $T_c$  effects, and negative  $R$  difference of EP-LP showed positive  
368  $T_c$  effect. The positive  $T_c$  anomaly of EP-LP reflected that the radiative process played the  
369 major role in the dormancy period. In the active growth time, the cooling effect of  $LH$   
370 partitioning dominated the  $T_c$  anomaly.



371  
372 **Fig.4** (a) The differences in the surface fluxes between the sowing scenarios of EP  
373 and LP, (b) its contributions to  $T_c$  anomaly.

374  $R_n$  means net radiation,  $T_a$  represents the temperature anomaly induced by changes  
375 in absorbed solar radiation.  $T_{LH}$  represents the temperature anomaly induced by changes  
376 in latent flux.  $T_{SH}$  represents the temperature anomaly induced by changes in sensible flux.  
377  $T_R$  represents the temperature anomaly induced by changes in residual term.  $T_S$  represents



378 the temperature anomaly induced by changes in solar radiation, latent, sensible and  
379 residual fluxes.

380

## 381 **4 Discussion**

### 382 **4.1 The diverse shift in sowing date of winter wheat in the NCP**

383 The spatiotemporal changes of winter wheat phenology had been examined. In the  
384 period of 1981-2009, sowing date delayed significantly at 13 station and advanced at 8  
385 stations out of the 36 agro-meteorological experiment stations (Xiao et al. 2013). In the  
386 NCP, the sowing date were on average delayed by 1.5 day/decade. The diverse trends in  
387 sowing date were also existed at the national scale, where 6 stations significantly  
388 advanced by up to 9.1 day/decade, and 11 stations significantly delayed by up to 10  
389 days/decade (Tao et al. 2012).

390 The main reasons for agricultural phenology shifts include climate warming and  
391 variety renewal (Mirschel et al. 2005; Eyshi Rezaei et al. 2017; Liu et al. 2017). Climate  
392 warming mainly leads to the delay of sowing date, and variety renewal is more likely to  
393 affect the length of reproductive period. The management practices, photoperiod, and the  
394 time of summer maize harvest also contributed to the shift of winter wheat sowing date  
395 (Yuan et al. 2010).

396 The proper sowing date is key to ensure winter wheat survived through winter and  
397 reduce the freezing injury, insect pests and other harmful conditions (Sacks et al. 2010;  
398 Zhang et al. 2012; Newbery et al. 2016). With faster growth in warmer environment, the  
399 sowing date should be postponed to maintain the proper coverage of winter wheat in  
400 dormancy period. The warming of the NCP is regionally consistent (Shi et al. 2014), and



401 the diverse change of sowing date will affect the coverage of winter wheat, especially one  
402 fifth stations advanced their sowing date. Earlier sowing may also benefited from the  
403 reduction in freezing damage and the increase in pest diseases caused by higher minimum  
404 temperature, since more above-ground biomass will not be subject to lethal freezing  
405 damage and will resist higher harms from pests and diseases. There are also management  
406 practices to counteract the effects of advanced sowing date, such as deep tillage and  
407 delayed irrigation, which reduce the development of leaves and stems.

408 Shifts in sowing date significantly affected land surface characteristic. And this  
409 affects probably more than we think especially in the early stage of winter wheat. As  
410 shown in Fig.5, there were several times of differences in surface coverage between the  
411 two sowing date. Differences in spectral characteristics, canopy structure and  
412 physiological activities between soil and winter wheat can significantly affect surface  
413 biophysical processes such as surface reflectivity, roughness, canopy resistance and  
414 surface energy budget (Richardson et al. 2013). In this study, the two sowing scenarios  
415 showed clear disparity in LAI (Fig.2a).



416

417 **Fig.5** Land surface characteristics of winter wheat in re-greening period for (a) early and  
418 (b) late sowing date



419

#### 420 **4.2 Warming effect of EP-LP in the dormancy period**

421 Although there were literatures reporting that the albedo process in winter is  
422 relatively important (Richardson et al. 2013; Lombardozzi et al. 2018), fewer studies  
423 directly addressed the influence of different surface characteristics and climate effect  
424 through biophysical process in the dormancy period. In the Oklahoma's winter wheat belt,  
425 the rapid crop growth during November exhibited a distinct cool anomaly against  
426 adjacent regions of dormant grassland. Over the period of December through April, the  
427 cool bias was visibly diminished although the greenness difference between grassland  
428 and wheat was more distinct (McPherson et al. 2004). The biophysical impacts between  
429 maize and perennial grass were simulated using Agro-IBIS model in US corn belt  
430 (Bagley et al. 2015). The results showed that much higher LAI of perennial scenario was  
431 existed in winter December–February ( $3$  vs  $0$   $\text{m}^2 \text{m}^{-2}$ ) and in summer June–August ( $10$  vs  
432  $4$   $\text{m}^2 \text{m}^{-2}$ ). Perennial grass had smaller surface albedo (coupling snow effect) than maize  
433 in winter, but showed quite small difference in summer. During winter and summer, the  
434 perennial scenario had slightly higher  $LH$  than the maize scenario, but the difference in  $R_n$   
435 between two scenarios was more than  $10\text{W m}^{-2}$  in winter (Bagley et al. 2015). The results  
436 of this current study indicate that higher LAI in winter has a warming effect, which is  
437 different from the conclusion above. The main reason was due to the relative  
438 contributions of surface albedo mechanism and surface flux distribution process.

439 Previous studies showed that the increase of vegetation cover caused warming  
440 feedback by destroying the high albedo of snow in the case of snow cover (Richardson et  
441 al. 2013; Bagley et al. 2015; Lombardozzi et al. 2018). But the simple increased crop

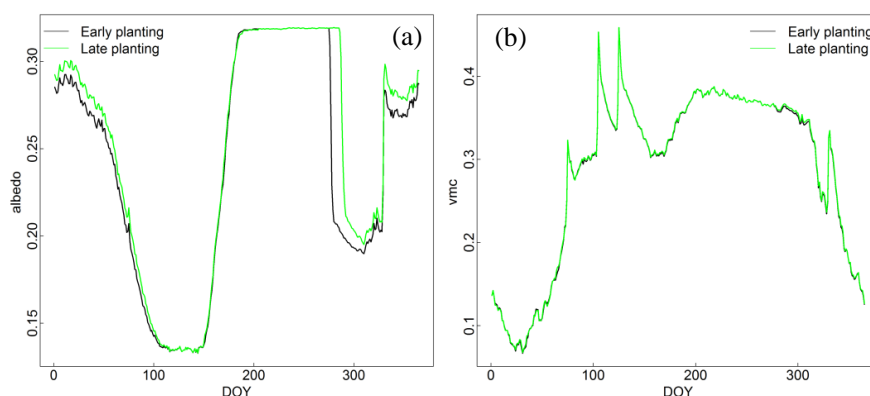


442 coverage in the bare ground would substantially alter surface albedo results from the  
443 decreasing contribution of the soil to the canopy reflectance (Hammerle et al. 2008). The  
444 soil reflectance is apparently high at our simulation (Fig.6a), which is favorable to the  
445 sharp reduction after crop covered. The measured surface albedo in winter could drop to  
446 0.14 (Liu et al. 2019). The surface albedo was computed based on surface energy budget  
447 at Weishan station, the bare ground albedo can be higher than 0.3 and the winter wheat  
448 lower than 0.15 (data not shown). Therefore, early sowing in EP scenario results in higher  
449 LAI, which can significantly affect the surface albedo at the initial stage and continuously  
450 have lower albedo than that in LP scenario. The effect of the soil on the canopy  
451 reflectance is negligible at  $LAI > 2 \text{ m}^2 \text{ m}^{-2}$  (Goudriaan 1977), which explained why the  
452  $R_n$  anomaly of EP-LP was small after the re-greening stage. In the model, the senescence  
453 of winter wheat is a process in which LAI decreases rapidly, and the disparity in LAI  
454 variations between the two scenarios further led to the difference in surface albedo and  $R_n$   
455 during the late growth period.

456 Low soil water content also contributed to the high surface albedo (Seneviratne et al.  
457 2010)(Fig.6b). With the decrease of surface soil moisture, surface albedo increased in  
458 winter, which explained why albedo in the winter was higher than that in the growth  
459 period. The increase in soil reflectivity caused by soil drying enhanced the role of low  
460 winter wheat reflectivity in surface albedo, the albedo disparity between the two  
461 scenarios increased in winter, so the albedo-radiative mechanism strengthened. Low soil  
462 moisture also contributed to the disparity in warming effect between EP and LP during  
463 dormancy period (Fig.6b). The lack of precipitation in winter made soil moisture unable  
464 to be replenished effectively, thus reducing soil evaporation and crop transpiration. But



465 during the growing season, soil moisture is high enough to supply transpiration. The  
466 lower the  $T_a$ , the lower the transpiration vitality, thus unable to offset the warming effect  
467 of increased  $R_n$  absorption, which explained why the winter  $T_c$  disparity among stations  
468 was controlled by  $T_a$ .



469 **Fig.6** Dynamics of (a) surface albedo and (b) surface soil moisture content under two  
470 sowing scenarios in winter wheat growing season  
471

472

### 473 4.3 Cooling effect of EP-LP during the growing period

474 The phenological shifts, such as earlier leaf unfolding, delayed leaf fall, and lengthening  
475 of the green-cover season have feedback on climate through biophysical and  
476 biogeochemical processes (Penuelas et al. 2009). Previous studies showed cooling effect  
477 in the photosynthetic active period through surface biophysical mechanism.

478 In the NCP, the increased spring surface greenness at farmland, benefited from  
479 advanced re-greening stage of winter wheat (Xiao et al. 2013; Liu et al. 2017), had  
480 cooling and wetting effects (Zhang et al. 2013) and suppressed the moderate to light  
481 rainfall (Zhang et al. 2015). The analysis found that surface greening increased the  
482 partitioning into  $LH$  and reduced  $SH$  to cooling surface air and suppression of rainfall



483 (Zhang et al. 2013; Zhang et al. 2015). Distinguished difference between early-covering  
484 crops (winter wheat, winter rapeseed, winter barley) and late-covering crops (corn, silage  
485 maize, sugar beet) in central Europe caused impacts on simulated surface energy fluxes  
486 and temperature in the Noah-MP model, the higher LAI led to an increase in  $LH$ ,  
487 decreased in  $SH$  and eventually surface cooling in May-September (Bohm et al. 2020).  
488 The Agro-IBIS model was used to study the impacts on surface energy balance of  
489 advanced corn sowing date (10 days): Early sowing means earlier development and  
490 senescence of LAI, causing stronger disparity of  $LH$  than  $R_n$  with bigger LAI and  
491 probably a slight cooling of  $T_a$  in June (Sacks and Kucharik 2011). Similar conclusions  
492 were presented based on simulated  $T_c$  results.

493

## 494 **5 Conclusions**

495 The dynamics of winter wheat LAI and  $T_c$  under two sowing date scenarios were  
496 simulated by the SiBcrop model in the NCP, and the  $T_c$  disparity between the two  
497 scenarios was explained by the surface energy balance. The findings include:

498 (1) Earlier sowing date of winter wheat had higher LAI than later sowing date.

499 (2) The  $T_c$  disparity between EP and LP is divided into two periods: warming effect  
500 in the dormancy period, and cooling effect in the active growth period.

501 (3) Surface energy balance can interpret the climate feedback mechanism of sowing  
502 date shift, that is, the dominated role of albedo-radiative process in the dormancy period  
503 is surpassed by  $LH$  partitioning-non-radiative process in the growth period.

504 (4) The responses of LAI and  $T_c$  to sowing date at station scale were divergent:  
505 controlled by  $T_a$  in the dormancy period, and influenced by  $P$  and  $T_a$  in the growth period.



506       The study had some shortcomings. The single model simulation was highly  
507 dependent on the structure and parameterization scheme of the model. The climate  
508 feedback was reflected by the canopy temperature. In the SiBcrop model, the spatial  
509 distribution of stations was not fully considered in the determination of sowing date,  
510 which resulted in too early or too late sowing at some stations.

511       Nevertheless, the study quantified the climate effects of the sowing date shift in  
512 winter dormancy period. The simulation error of sowing date in land surface models is  
513 commonly higher than 10 days (Song et al. 2013; Chen et al. 2020), which may produce  
514 detectable climate effect especially in northern winter and then misestimate the variation  
515 of minimum temperature. The findings showed that even when land use/cover type  
516 remains unchanged, variations in surface properties caused by sowing date might still  
517 have detectable climatic effects by affecting the surface biophysical process. The  
518 conclusion implies that we need to consider not only conversions of land use/cover types  
519 but also changes in crop management to understand climate change.

520

## 521 **Acknowledgments**

522       This study is supported by the National Natural Science Foundation of China  
523 (41801020).

524

## 525 **References**

526 Bagley, J. E., Kueppers, L. M., Billesbach, D. P., Williams, I. N., Biraud, S. C., and Torn,  
527 M. S.: The influence of land cover on surface energy partitioning and evaporative fraction



528 regimes in the US Southern Great Plains. *Journal of Geophysical Research-Atmospheres*,  
529 122(11), 5793-5807, 2017.

530 Bagley, J. E., Miller, J., and Bernacchi, C. J.: Biophysical impacts of climate - smart  
531 agriculture in the Midwest United States. *Plant, cell & environment*, 38(9), 1913-1930,  
532 2015.

533 Bohm, K., Ingwersen, J., Milovac, J., and Streck, T.: Distinguishing between early- and  
534 late-covering crops in the land surface model Noah-MP: impact on simulated surface  
535 energy fluxes and temperature. *Biogeosciences*, 17(10), 2791-2805, 2020.

536 Boisier, J. P., de Noblet-Ducoudre, N., Pitman, A. J., Cruz, F. T., Delire, C., van den  
537 Hurk, B. J. J. M., et al.: Attributing the impacts of land-cover changes in temperate  
538 regions on surface temperature and heat fluxes to specific causes: Results from the first  
539 LUCID set of simulations. *Journal of Geophysical Research-Atmospheres*, 117, 2012.

540 Chen, M., Griffis, T. J., Baker, J., Wood, J. D., and Xiao, K.: Simulating crop phenology  
541 in the Community Land Model and its impact on energy and carbon fluxes. *Journal of*  
542 *Geophysical Research-Biogeosciences*, 120(2), 310-325, 2015.

543 Chen, Y., liu, F., Tao, F., Ge, Q., Jiang, M., Wang, M., et al.: Calibration and validation  
544 of SiBcrop Model for simulating LAI and surface heat fluxes of winter wheat in the  
545 North China Plain. *Journal of Integrative Agriculture*, 19(9), 2-11, 2020.

546 Cho, M. H., Boo, K. O., Lee, J., Cho, C., and Lim, G. H.: Regional climate response to  
547 land surface changes after harvest in the North China Plain under present and possible  
548 future climate conditions. *Journal of Geophysical Research-Atmospheres*, 119(8),  
549 4507-4520, 2014.



550 Collatz, G. J., Berry, J. A., Farquhar, G. D., and Pierce, J.: The relationship between the  
551 Rubisco reaction mechanism and models of photosynthesis\*. *Plant, Cell & Environment*,  
552 13(3), 219-225, 1990.

553 Cooley, H. S., Riley, W. J., Torn, M. S., and He, Y.: Impact of agricultural practice on  
554 regional climate in a coupled land surface mesoscale model. *Journal of Geophysical  
555 Research Atmospheres*, 110(D03113, doi:10.1029/2004JD005160.), -, 2005.

556 Cui, J., Yan, P., Wang, X., Yang, J., Li, Z., Yang, X., et al.: Integrated assessment of  
557 economic and environmental consequences of shifting cropping system from  
558 wheat-maize to monocropped maize in the North China Plain. *Journal of Cleaner  
559 Production*, 193, 524-532, 2018.

560 Eyshi Rezaei, E., Siebert, S., and Ewert, F.: Climate and management interaction cause  
561 diverse crop phenology trends. *Agricultural and Forest Meteorology*, 233, 55-70, 2017.

562 Falge, E., Baldocchi, D., Olson, R., Anthoni, P., Aubinet, M., Bernhofer, C., et al.: Gap  
563 filling strategies for defensible annual sums of net ecosystem exchange. *Agricultural and  
564 Forest Meteorology*, 107(1), 43-69, 2001.

565 Farquhar, G. D., von Caemmerer, S., and Berry, J. A.: A biochemical model of  
566 photosynthetic CO<sub>2</sub> assimilation in leaves of C<sub>3</sub> species. *Planta*, 149(1), 78-90, 1980.

567 Goudriaan, J. 1977. *Crop micrometeorology : a simulation study*, Pudoc.

568 Hammerle, A., Haslwanter, A., Tappeiner, U., Cernusca, A., and Wohlfahrt, G.: Leaf area  
569 controls on energy partitioning of a temperate mountain grassland. *Biogeosciences*, 5(2),  
570 421-431, 2008.



571 Jeong, S.-J., Ho, C.-H., Piao, S., Kim, J., Ciais, P., Lee, Y.-B., et al.: Effects of double  
572 cropping on summer climate of the North China Plain and neighbouring regions. *Nature*  
573 *Clim. Change*, 4(7), 615-619, 2014.

574 Lei, H., Yang, D., Lokupitiya, E., and Shen, Y.: Coupling land surface and crop growth  
575 models for predicting evapotranspiration and carbon exchange in wheat-maize rotation  
576 croplands. *Biogeosciences*, 7(10), 3363-3375, 2010.

577 Liu, C., Gao, Z., Li, Y., Gao, C. Y., Su, Z., and Zhang, X.: Surface Energy Budget  
578 Observed for Winter Wheat in the North China Plain During a Fog–Haze Event.  
579 *Boundary-Layer Meteorology*, 170(3), 489-505, 2019.

580 Liu, F., Chen, Y., Shi, W., Zhang, S., Tao, F., and Ge, Q.: Influences of agricultural  
581 phenology dynamic on land surface biophysical process and climate feedback. *Journal of*  
582 *Geographical Sciences*, 27(9), 1085-1099, 2017.

583 Liu, S., Xu, Z., Zhu, Z., Jia, Z., and Zhu, M.: Measurements of evapotranspiration from  
584 eddy-covariance systems and large aperture scintillometers in the Hai River Basin, China.  
585 *Journal of Hydrology*, 487, 24-38, 2013.

586 Liu, S. M., Xu, Z. W., Wang, W. Z., Jia, Z. Z., Zhu, M. J., Bai, J., et al.: A comparison of  
587 eddy-covariance and large aperture scintillometer measurements with respect to the  
588 energy balance closure problem. *Hydrology and Earth System Sciences (HESS) &*  
589 *Discussions (HESSD)*, 15, 1291-1306, 2011.

590 Liu, Y. A., Wang, E. L., Yang, X. G., and Wang, J.: Contributions of climatic and crop  
591 varietal changes to crop production in the North China Plain, since 1980s. *Global Change*  
592 *Biology*, 16(8), 2287-2299, 2010.



593 Liu, Y. J., Chen, Q. M., Ge, Q. S., Dai, J. H., Qin, Y., Dai, L., et al.: Modelling the  
594 impacts of climate change and crop management on phenological trends of spring and  
595 winter wheat in China. *Agricultural and Forest Meteorology*, 248, 518-526, 2018.

596 Liu, Z., Wu, C., Liu, Y., Wang, X., Fang, B., Yuan, W., et al.: Spring green-up date  
597 derived from GIMMS3g and SPOT-VGT NDVI of winter wheat cropland in the North  
598 China Plain. *Isprs Journal of Photogrammetry & Remote Sensing*, 130, 81-91, 2017.

599 Lokupitiya, E., Denning, S., Paustian, K., Baker, I., Schaefer, K., Verma, S., et al.:  
600 Incorporation of crop phenology in Simple Biosphere Model (SiBcrop) to improve  
601 land-atmosphere carbon exchanges from croplands. *Biogeosciences*, 6(6), 969-986, 2009.

602 Lombardozzi, D. L., Bonan, G. B., Wieder, W., Grandy, A. S., Morris, C., and Lawrence,  
603 D. M.: Cover Crops May Cause Winter Warming in Snow - Covered Regions.  
604 *geophysical research letters*, 45(18), 9889-9897, 2018.

605 Mahdi, L., Bell, C. J., and Ryan, J.: Establishment and yield of wheat (*Triticum turgidum*  
606 L.) after early sowing at various depths in a semi-arid Mediterranean environment. *Field*  
607 *Crops Research*, 58(3), 187-196, 1998.

608 Mahmood, R., Pielke, R. A., Hubbard, K. G., Niyogi, D., Dirmeyer, P. A., McAlpine, C.,  
609 et al.: Land cover changes and their biogeophysical effects on climate. *International*  
610 *Journal of Climatology*, 34(4), 929-953, 2014.

611 McPherson, R. A., Stensrud, D. J., and Crawford, K. C.: The Impact of Oklahoma's  
612 Winter Wheat Belt on the Mesoscale Environment. *Monthly Weather Review*, 132(2),  
613 405-421, 2004.



- 614 Mirschel, W., Wenkel, K.-O., Schultz, A., Pommerening, J., and Verch, G.: Dynamic  
615 phenological model for winter rye and winter barley. *European Journal of Agronomy*,  
616 23(2), 123-135, 2005.
- 617 Najeeb, U., Bange, M. P., Atwell, B. J., and Tan, D. K. Y.: Low Incident Light Combined  
618 with Partial Waterlogging Impairs Photosynthesis and Imposes a Yield Penalty in Cotton.  
619 *Journal of Agronomy and Crop Science*, 202(4), 331-341, 2016.
- 620 Newbery, F., Qi, A., and Fitt, B. D.: Modelling impacts of climate change on arable crop  
621 diseases: progress, challenges and applications. *Current Opinion in Plant Biology*, 32,  
622 101-109, 2016.
- 623 Penuelas, J., Rutishauser, T., and Filella, I.: Phenology Feedbacks on Climate Change.  
624 *Science*, 324(5929), 887-888, 2009.
- 625 Reynolds, M., Foulkes, J., Furbank, R., Griffiths, S., King, J., Murchie, E., et al.:  
626 Achieving yield gains in wheat. *Plant Cell and Environment*, 35(10), 1799-1823, 2012.
- 627 Richardson, A. D., Keenan, T. F., Migliavacca, M., Ryu, Y., Sonnentag, O., and Toomey,  
628 M.: Climate change, phenology, and phenological control of vegetation feedbacks to the  
629 climate system. *Agricultural and Forest Meteorology*, 169, 156-173, 2013.
- 630 Sacks, W. J., Deryng, D., Foley, J. A., and Ramankutty, N.: Crop planting dates: an  
631 analysis of global patterns. *Global Ecology and Biogeography*, 19(5), 607-620, 2010.
- 632 Sacks, W. J., and Kucharik, C. J.: Crop management and phenology trends in the US  
633 Corn Belt: Impacts on yields, evapotranspiration and energy balance. *Agricultural and*  
634 *Forest Meteorology*, 151(7), 882-894, 2011.
- 635 Schillinger, W. F.: Rainfall Impacts Winter Wheat Seedling Emergence from Deep  
636 Planting Depths. *Agronomy Journal*, 103(3), 730, 2011.



637 Seneviratne, S. I., Corti, T., Davin, E. L., Hirschi, M., Jaeger, E. B., Lehner, I., et al.:  
638 Investigating soil moisture–climate interactions in a changing climate: A review.  
639 *Earth-Science Reviews*, 99(3), 125-161, 2010.

640 Seneviratne, S. I., Phipps, S. J., Pitman, A. J., Hirsch, A. L., Davin, E. L., Donat, M. G.,  
641 et al.: Land radiative management as contributor to regional-scale climate adaptation and  
642 mitigation. *Nature Geoscience*, 11(2), 88-96, 2018.

643 Shi, P., Sun, s., Wang, M., Li, N., Wang, J., Jin, Y., et al.: Climate change regionalization  
644 in China (1961 - 2010)(In Chinese). *Science China: Earth Sciences*, 44(10), 2294-2306,  
645 2014.

646 Song, Y., Jain, A. K., and McIsaac, G. F.: Implementation of dynamic crop growth  
647 processes into a land surface model: evaluation of energy, water and carbon fluxes under  
648 corn and soybean rotation. *Biogeosciences*, 10(12), 8201-8201, 2013.

649 Tao, F., Yokozawa, M., and Zhang, Z.: Modelling the impacts of weather and climate  
650 variability on crop productivity over a large area: A new process-based model  
651 development, optimization, and uncertainties analysis. *Agricultural and Forest  
652 Meteorology*, 149(5), 831-850, 2009.

653 Tao, F. L., Zhang, S., Zhang, Z., and Rotter, R. P.: Maize growing duration was  
654 prolonged across China in the past three decades under the combined effects of  
655 temperature, agronomic management, and cultivar shift. *Global Change Biology*, 20(12),  
656 3686-3699, 2014.

657 Tao, F. L., Zhang, S. A., and Zhang, Z.: Spatiotemporal changes of wheat phenology in  
658 China under the effects of temperature, day length and cultivar thermal characteristics.  
659 *European Journal of Agronomy*, 43, 201-212, 2012.



- 660 Wuest, S. B.: Tillage depth and timing effects on soil water profiles in two semiarid soils.  
661 Soil Science Society of America Journal, 74(5), 1701-1711, 2010.
- 662 Wutzler, T., Lucas-Moffat, A., Migliavacca, M., Knauer, J., Sickel, K., Šigut, L., et al.:  
663 Basic and extensible post-processing of eddy covariance flux data with REddyProc.  
664 Biogeosciences, 15(16), 5015-5030, 2018.
- 665 Xiao, D. P., Moiwo, J. P., Tao, F. L., Yang, Y. H., Shen, Y. J., Xu, Q. H., et al.:  
666 Spatiotemporal variability of winter wheat phenology in response to weather and climate  
667 variability in China. Mitigation and Adaptation Strategies for Global Change, 20(7),  
668 1191-1202, 2015.
- 669 Xiao, D. P., and Tao, F. L.: Contributions of cultivars, management and climate change  
670 to winter wheat yield in the North China Plain in the past three decades. European  
671 Journal of Agronomy, 52, 112-122, 2014.
- 672 Xiao, D. P., Tao, F. L., Liu, Y. J., Shi, W. J., Wang, M., Liu, F. S., et al.: Observed  
673 changes in winter wheat phenology in the North China Plain for 1981-2009. International  
674 Journal of Biometeorology, 57(2), 275-285, 2013.
- 675 Yuan, L., Wang, E., Yang, X., and Jing, W.: Contributions of climatic and crop varietal  
676 changes to crop production in the North China Plain, since 1980s. Global Change  
677 Biology, 16(8), 2287-2299, 2010.
- 678 Zhang, X., Huang, G., Huang, Z., Bian, X., and Jiang, X.: Effects of low temperature on  
679 freezing injury of various winter wheat cultivars at different sowing time. Agricultural  
680 Science & Technology, 13(11), 2332-2337, 2012.



681 Zhang, X., Tang, Q., Zheng, J., Ge, Q., and Mao, R.: Suppression of spring rain by  
682 surface greening over North China Plain. *International Journal of Climatology*, 35(10),  
683 2752-2758, 2015.

684 Zhang, X. Z., Tang, Q. H., Zheng, J. Y., and Ge, Q. S.: Warming/cooling effects of  
685 cropland greenness changes during 1982-2006 in the North China Plain. *Environmental*  
686 *Research Letters*, 8(2), 2013.

687